DYNAMICS OF DENSE PYROCLASTIC FLOWS ON VENUS – INSIGHTS INTO PYROCLASTIC ERUPTIONS. I. Ganesh[1] (indujaa@email.arizona.edu), L. McGuire[2] and L.M. Carter[1] [1]Department of Planetary Sciences, University of Arizona, [2]Department of Geosciences, University of Arizona.

Introduction: Volcanic and coronal summit deposits having feathery margins and lacking definitive flow features on Venus have been proposed to be pyroclastic flow deposits [1-3]. Their radar properties include high backscatter, high circular polarization ratio (CPR) and low-moderate degree of linear polarization as noted from Magellan and Arecibo radar data [1]. Based on superposition relationships, they appear to be the youngest deposits in the region [1,2]. The flows had long runouts from the source (60-120 km) akin to large ignimbrite eruptions on Earth that are not observed in current times [4-8]. These observations hint at the presence of localized volatile-rich magma reservoirs which fed young pyroclastic eruptions. Understanding the characteristics of pyroclastic flows responsible for emplacing these deposits will provide insights into the style and mechanics of possible pyroclastic eruptions on Venus. Here, we use 2D mass flow models to simulate pyroclastic flow dynamics and constrain the properties of the eruption that produced the observed deposits.

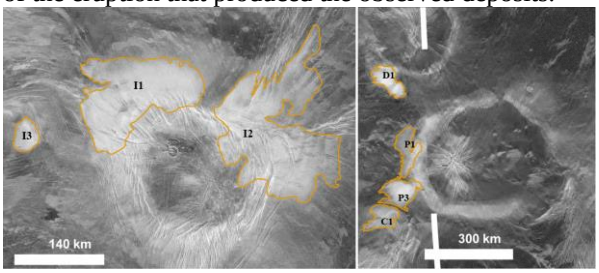

Fig. 1: Magellan SAR image of Irnini Mons (left), and Pavlova and Didilia corona (right). Radar-bright diffuse deposits from [1] have been mapped in yellow.

Proposed pyroclastic deposits: We focus our modeling efforts on long runout deposits at the summit of Irnini and Anala Mons in Western Eistla Regio and on the flanks of Didilia and Pavlova Corona in Eastern Eistla Regio (Fig 1). We use ~100 m/pix Magellan SAR data to map the deposits. Stereo-SAR topography [9] of 1-2 km/pix resolution was used for determining the surface elevation and slope in the area. The average slope is < 2° at all deposits.

Numerical model: We solve depth-averaged shallow water equations on a 2D topographical grid to simulate initiation and transport of a dense, particle-laden pyroclastic flow [10]. The flow is modeled as a mixture of solids (ash, pumice and lithics) suspended in a Newtonian fluid, the propagation of which is driven by topography, and retarded by basal friction and viscous resistance. This approach is often used for modeling fluidized mass flows with high volume fraction of solids (20 – 40 %) [11, 12], thereby making it suitable for deposits in our study area where cm-sized clasts embedded in the deposit are thought to give rise to high radar backscatter and high CPR. Following previous studies, our model uses a 1st order Godunov scheme with an HLLC Riemann solver to calculate the flux across the grid cell interfaces; the source terms are solved separately using an explicit Euler method.

Initiation mechanisms: We model pyroclastic flows formed by two different mechanisms: column collapse and fountaining. The column collapse initiation mechanism is simulated by allowing a cylindrical column of user-defined dimensions to collapse at time $t = 0$ and flow under gravity. Multiple columns of equal volume are initialized along the circumferential summit structures to represent spatiotemporally distributed eruptions. For the fountain fed flow case, a continuous string of cells above the upper margin of the deposit are assumed to represent feeding cells with a constant eruption rate (expressed in ms^{-1}) until time $t \leq t_{fountain}$. We perform simulations with a range of collapse heights for collapse-fed flows, different fountaining duration and eruption rates for fountain-fed flows, and varying pore fluid pressure for both cases to study how these parameters affect final flow runout and deposit thickness.

Initiation	Collapse	Fountaining
Collapse height (km)	100	-
Eruption rate (ms^{-1})	-	25
Fountain duration (s)	-	500
Initial pore fluid pressure	0.99	0.99

Table 1: Parameters used for model results in Fig 2.

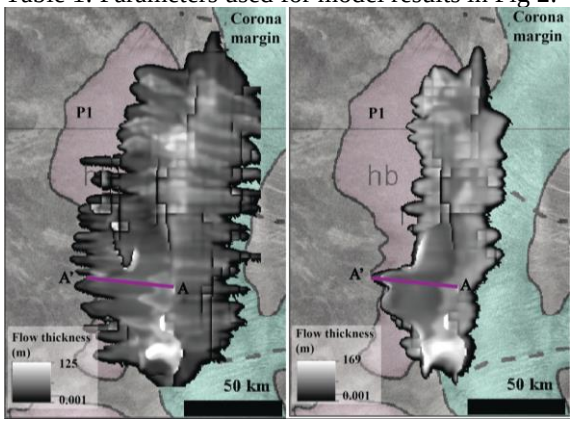

Fig 2: Modeled flow thickness and runout for deposit P1 using parameters listed in table 1 for collapse initiation (left) and fountaining initiation (right).

Results and discussion: Deposit P1 is used as a representative example to discuss trends in the model results that were found to be common to all the modeled deposits. Final flow thicknesses and runout at P1 for both styles of initiation using parameters listed in Table

1 are shown in Fig 2. The maximum runout observed is ~ 45 km for fountain fed flows; for collapse-fed flows of equivalent volume, we see runouts as high as ~ 55 km. The higher flow velocity imparted by large collapse heights favors longer flow distances when compared to flows that are initiated from low fountaining.

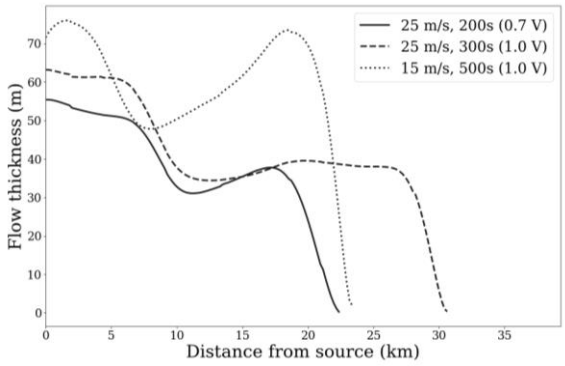

Fig 3: Flow thickness along A-A' for different eruption rates and duration. The dashed and dotted curves represent flow volume = 249 km^3. The solid curve shows a smaller flow of volume 166 km^3.

We investigate model sensitivity to parameters such as collapse height, eruption rate, fountaining duration and pore fluid pressure by comparing flow properties along the transect A-A' (Fig 2) for different combinations of input parameters. Fig 3 shows the change in flow thickness and runout as a function of change in influx duration and eruption rate (expressed in ms^{-1}). For the same flow volume (1.0 V), flows fed by a higher rate over shorter durations (dashed curve) have longer runouts compared to long-lived eruptions with smaller rate (dotted curve). While longer eruptions lead to extrusion of more volume available for the flow, our simulations show a 'pile-up' effect owing to quick deceleration of the flow along shallow slopes. It is also notable that a smaller flow (0.7 V, solid curve) fed by higher rates has similar runout to the larger flow (dotted curve) fed by long eruptions.

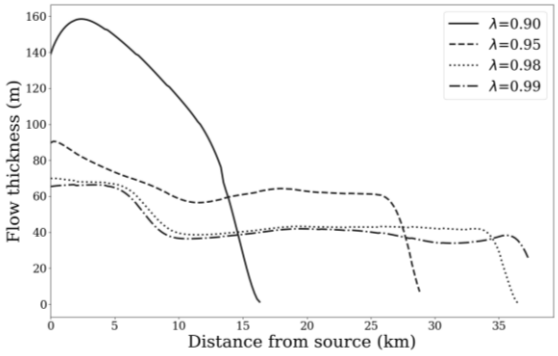

Fig 4: Flow thickness along A-A' for different starting pore pressure percentages. High pore pressure increases mobility and induces longer runout.

Fig 4 shows the effect of changes in pore fluid pressure on the final runout along A-A' for fountain-fed flows. A high ratio of pore pressure to basal normal stress (λ>0.95) is necessary to produce long runouts. Greater pore fluid pressure boosts runout by reducing interparticle friction. Given typical values for the basal friction angle of pyroclastic flows and the relatively low slopes at our study site, high pore pressure becomes critical for maintaining flow mobility.

Fig 5 shows the changes in runout along A-A' as a function of column collapse height for collapse fed flows. Predictably, higher collapse heights impart more kinetic energy to the flow, leading to greater runout.

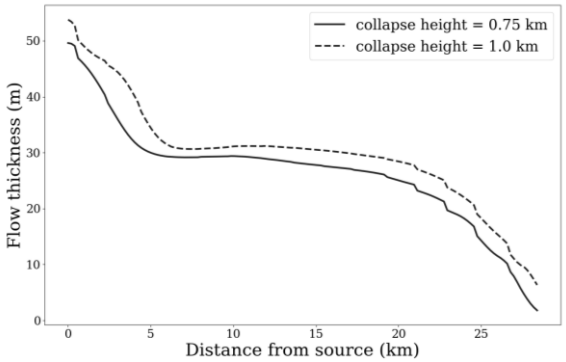

Fig 5: Flow thickness along A-A' for column collapse height. Higher collapse heights result in longer flows.

Conclusions and future work: Large pyroclastic flows from distributed sources are necessary to emplace long and laterally extensive deposits like those possibly identified on Venus. Columns which collapse from a great height or sustained fountains with high eruption rates can give rise to such voluminous flows. For flows formed by both mechanisms, high pore fluid pressure is required to sustain mobility and achieve longer runouts.

Going forward, we will explore turbulence driven pyroclastic flows which are thought to have emplaced large deposits like the Taupo ignimbrite on Earth [13].

Acknowledgments: This study was supported by a FINESST award to I. Ganesh and an SSW grant to L. M. Carter. Magellan data was processed using USGS Astrogeology Science Center's Map-A-Planet 2.

References: [1] Campbell B. A. et al. (2017) JGR 122, 1580–1596. [2] Grosfils E. B. et al. (2011), *USGS Sci. Inv. Map 3121*. [3] Ghail R. C. and Wilson. L. (2015) *Geological Soc. Lond. Spl. Pub. 401*. [4] Roche, O. et al. (2016) *Nat. Comm.* 7:10890. [5] Wilson, C. J. N. et al. (1995) *Nature 378*, 605–607. [6] Streck M. J. and Grunder A. L. (1995) *Bull Volcanol 57*, 151-169. [7] Henry C. D. et al. (2012) *Geosphere 8*, 1-27. [8] Branney, M. J. and Kokelaar, P. (2002) *Geological Soc. Lond. Mem.* 27. [9] Herrick, R. R. et al. (2012) *EOS Trans. AGU 93*, 125-126. [10] Iverson R. M. and Denlinger R. P. (2001) *JGR, 106*, 537-552. [11] Patra A. K. et al. (2005) *JVGR 139*, 1–22. [12] Sheridan M. F. et al. (2005) *JVGR 139*, 89–102. [13] Bursik M. I. and Woods A. W. (1996) Bull Volcanol 58, 175-193.